High dynamic range, hyper-terahertz detection with silicon photoconductors

A. C. Muir[1], A. Hussain[2] and S. R. Andrews[1a]

[1]Department of Physics, University of Bath, Bath BA2 7AY, UK

[2] STFC, Rutherford Appleton Laboratory, Didcot OX11 0QX, UK

Abstract

The frequency response of ion implanted silicon photoconductors for detection in time domain terahertz spectroscopy has been studied between 0.2 and 30 THz. Unlike devices using polar photoconductors or ones having polar substrates, which have a complicated response spectrum in the region of their restrahlen bands, the response of silicon detectors fabricated on silicon substrates is relatively featureless. When used with amplified laser systems the dynamic range of Si detectors is shown to be very similar to GaAs devices with the same geometry over a 20 THz range, superior to air biased coherent detection (ABCD) at frequencies below ~7 THz and comparable with both ABCD and electro-optic sampling in thin ZnTe crystals between 7 and 20 THz. Together with their ease of use and linear response to terahertz fields approaching 1 MV/cm, this suggests that Si photoconductors could be a competitive choice for sensitive detection in nonlinear hyper-terahertz spectroscopy.

PACS numbers 07.57.Kp, 73.61.Ey, 78.47.+p, 78.66.Fd, 84.40.Ba

a) e-mail address: s.r.andrews@bath.ac.uk

Time domain terahertz spectroscopy (TDTS), which exploits femtosecond near infrared lasers to both generate and detect pulses of far infrared radiation using all-optical or electro-optical techniques has become a widely used experimental tool in the past two decades [1]. Applications range from materials characterization to industrial quality control and security screening [1]. In most laboratory TDTS systems the bandwidth is ~3 THz and the THz pulses have very low energies of order 100 fJ and are a coherently sampled using photoconducting antennas or electro-optic crystals gated by probe pulses split off from the pump pulse used to

generate the THz radiation. The useful system bandwidth is typically ~3 THz but recently there has been increasing activity in extending coherent generation and detection techniques to frequencies in the tens of THz and to much higher THz pulse energies in the μJ range for nonlinear solid state spectroscopy [3]. In what follows we define the term hyper-THz to mean the extended frequency range from roughly 0.1 THz to 30 THz, which encompasses the majority of sub-bandgap excitations in condensed matter.

The first detectors used in TDTS were based on photoconductive antennas fabricated in ion implanted silicon on sapphire (SOS) [4,5] but the commercial availability of low temperature (LT) grown GaAs with higher mobility and sub-picosecond carrier lifetime without further processing has led to it becoming the most commonly used material [1]. Although short carrier lifetime is required for low noise, it has only a small effect on bandwidth [5] and for sufficiently short optical sampling pulses, detection using GaAs has been shown to be possible for frequencies in the mid-infrared [5,6]. In a previous paper [7] we reported a study of the multi-THz response and dynamic range of As^+ implanted and LT GaAs photoconductive receivers in which we concluded that the two materials are similar in offering a dynamic range that is competitive with the common alternative technique of electro-optic sampling (EOS) in ZnTe [8]. The usefulness of coherent detection schemes based on polar materials such as GaAs or ZnTe is however constrained by the difficulty of making quantitative measurements at frequencies in the vicinity of their restrahlen bands where there is strong absorption and dispersion associated with the coupling of light to polar optical phonons. In this letter we explore the potential of Si, a non-polar photoconductive material, for hyper-THz detection and make a comparison with GaAs photoconductors, EOS and the recently introduced broadband technique known as air biased coherent detection (ABCD) [9].

The three photoconductive receivers that were studied were made from polycrystalline silicon on oxide (SOX) grown by low-pressure chemical vapour deposition, commercial silicon on sapphire (SOS) and GaAs grown by molecular beam epitaxy. The SOX wafer comprised a 1.1 μm thick Si layer on a high resistivity Si substrate with an intervening 0.6 μm thick layer of thermal oxide and is similar to ones described previously at low THz frequencies [10,11]. The SOS wafer consisted of 0.6 μm of Si on sapphire and the GaAs wafer of 1 μm of GaAs on 100 nm of AlAs on semi-insulating GaAs. All samples were ion implanted to achieve sub-ps photoexcited carrier lifetimes and high average resistivity under optical gating conditions. The GaAs and SOS wafers were respectively As^+ and O^+ implanted as described in references 7 and

12. The SOX was O^+ implanted at 75, 150, 280 and 500 keV with doses in the ratio 1.24:1.86:2.49:3 so as to obtain an approximately uniform vacancy concentration over the depth of the epilayer at a total dose of $3x10^{14}$ cm^{-2}. The carrier lifetimes determined by time resolved optical reflectivity (SOX, SOS) and optical pump-THz probe (GaAs) measurements were 670±50 fs (SOX), 430±30 fs (SOS) and 450±50 fs (GaAs). With the chosen implantation doses the dark resistivity of all three photoconductors was in the range 50-100 kΩcm.

THz receivers were manufactured with a simple surface electrode geometry consisting of a pair of parallel 10 μm wide, 10 mm long Ti:Au tracks separated by 50 μm. Plasma etching was used to remove the active layer from between the tracks except for a central 50x50 μm photoswitch region and the dark resistances of all devices exceeded 500 MΩ. The devices were characterised using unamplified, 74 MHz repetition rate and amplified, 2 kHz repetition rate Ti:sapphire laser systems with wavelengths of 800 nm. In the first system 4 nJ, 12 fs pump pulses were used to create THz radiation via transient diffusion currents in n-type InAs (doped at 10^{17} cm^{-3}) or optical rectification in phase matched GaSe. THz pulses co-propagating with a sampling beam of 0.5 nJ, 800 nm pulses were focused onto the front surface of the photoconducting devices using a 100 mm effective focal length, 90° off-axis parabolic mirror. Residual pump light was blocked by a 500 μm thick, high resistivity Si filter. In the second system 1.5 mJ, 35 fs pump pulses were frequency doubled in a 100 μm thick β-BBO crystal and the resulting two colour radiation was used to generate intense (~150 nJ), ~20 THz bandwidth pulses in an air-plasma filament [13]. The generation efficiency was optimised by means of a dual colour half-wave plate, phase matching with the aid of a pair of fused silica wedges and compensation for the group delay in these components using an α-BBO timing plate [13]. The photoconductive detection geometry was similar to that described earlier except that the gating pulses were much higher in energy (80 nJ compared with 0.5 nJ) and an additional, 500 μm thick, intrinsic Ge filter was used to prevent long wavelength continuum light generated in the plasma from reaching the detector. In both systems the pump was mechanically chopped at 1 kHz and the signal current was detected using a lock-in amplifier. Time domain data was typically obtained by averaging 250 delay line scans acquired at 0.5 Hz with a lock-in time constant of 1 ms.

Examples of time domain receiver signals and their corresponding spectra for the GaAs and SOX devices obtained using the low energy laser system are shown in Fig. 1. In Figs. 1(a) and 1(c) differences between the two devices can be mainly attributed to the coupling of light to the

LO phonon in GaAs (long lived oscillations in Fig. 1(a), sharp peak near 8.7 THz in Fig. 1(c)). In Figs. 1(b) and 1(d) the THz spectrum does not significantly overlap the restrahlen band of GaAs so that the time domain traces and spectra of the SOX and GaAs receivers have almost the same shape. The terahertz source spectra are not known well enough to allow deconvolution of the receiver frequency response from the measured spectra but the ratio of the response spectrum of one receiver to another can provide insight into the behaviour. The ratio spectra for SOX and SOS using GaAs as the reference are shown in Figs. 2(a) and 2(b) respectively. The THz induced photocurrent at frequency ω is proportional to $E(\omega)n(\omega)t(\omega)\mu(\omega)$ where E is the component of the incident THz electric field polarized perpendicular to the electrodes, n is the spectrum of the time varying carrier density generated by the sampling pulse, μ is the photoexcited electron mobility and t is the amplitude transmission coefficient of the device surface [7]. The parameter t is determined by the dielectric functions and thicknesses of the different material layers. An additional, photoexcited plasma contribution to t gives rise to screening of the THz field at high gating powers which leads to saturation of the detected photocurrent. The carrier trapping times in all the devices are a significant fraction of a picosecond so that only t and μ control the shape of the ratio spectra at frequencies higher than a few THz. The signatures of optical phonons in GaAs and AlAs on t are clear in Fig. 2(a). The peak at 8.0 THz and dip at 8.7 THz correspond to minima and maxima in the reflectivity spectrum of GaAs near the TO and LO phonon frequencies respectively, whilst the peak near 10.9 THz is related to the TO phonon in the underlying AlAs. The response ratio for SOS, shown in Fig. 2(b), is similar to that of SOX below 12 THz but at higher frequencies the spectrum is strongly modified by the effect on the sapphire reflectivity of four infrared-active E_u symmetry vibrational modes with frequencies of 11.5, 13.1, 17.1, and 19.1 THz [14,15]. This shows the importance of choosing a non-polar substrate.

The overall decrease in response ratio by a factor of 4 or 5 with increasing ω in figures 2(a) and 2(b) reflects the different frequency dependence of the mobilities of ion implanted Si and GaAs. The mobility of the As^+ implanted GaAs was found to be 1500±300 cm^2/Vs near 1 THz using the same optical pump-THz probe measurements used to determine the photocarrier lifetime and is similar to that previously observed in LT GaAs [16]. The mobility near 1 THz in implanted Si films has previously been found to be ~400 cm^2/Vs [17], in rough agreement with the value of ~300 cm^2/Vs deduced for both SOS and SOX films from the order of magnitude difference in sensitivity of the Si and GaAs devices near 1 THz at very low sampling power

where field screening can be neglected. In making this comparison we have accounted for the different experimentally determined absorption coefficients of ion implanted Si and GaAs at 800 nm of $5x10^3$ cm^{-1} and $2x10^4$ cm^{-1} respectively. If the electron conductivity masses in GaAs and Si are taken as $0.067m_e$ and $0.29m_e$ respectively then we infer that the mobility scattering time, τ, in the two materials has roughly the same value of ~50 fs. In a Drude-like model the mobility can be expressed as $\mu(\omega) \approx \mu(0)/(1+i\omega\tau)$, where $\mu(0) = e\tau/m$ and m is the electron conductivity effective mass. In this model we therefore expect that the Si to GaAs response ratio in Figs. 2(a) and 2(b) be equal to the electron conductivity mass ratio of 0.23 at both low and high frequency, which is inconsistent with the overall decrease in ratio with increasing frequency. There are two plausible modifications to the Drude model that might account for the discrepancy. The first is to assume a distribution of scattering times, as for example, is implicit in the Cole-Davidson conductivity model [18] in which the mobility is expressed as $\mu(\omega) = \mu(0)/(1+i\omega\tau)^{\beta}$. If the phenomenological parameter β for the implanted GaAs is smaller than for Si then the response ratio decreases with increasing ω, as observed although the difference in β of ~0.45 required to give a reasonable fit to the data (model curve in Fig. 2(a)) is too large to be realistic. The second modification is to take into account band non-parabolicity and the fact that sampling pulses excite electrons with an excess energy is ~0.3 eV in Si so that the initial conductivity effective mass is ~$0.4m_e$. Energy relaxation then leads to a decrease to the band edge value of $0.29m_e$ on a time scale of a few hundred fs [19,20]. A similar, although much smaller effect occurs in GaAs. On short time scale the mobility might therefore be expected to be lower than on long time scales and thus decrease with increasing frequency. This effect should be a larger in Si than in GaAs, as required to explain the trends in Figs. 2(a) and 2(b).

Fig. 3 shows time domain traces and spectra obtained at the larger THz and sampling pulse energies possible using the amplified laser system. The dips in the spectra near 10.5 and 19 THz are due to multiphonon absorption in the Ge and Si filters. The signal current increased linearly with probe pulse energies up to 20 nJ in the Si devices and 5 nJ in GaAs but sub-linearly at higher energies because the photoexcited carrier densities are then sufficient to noticeably screen the THz field. The peak focused THz field at 9 THz was estimated to be 0.7 ± 0.2 MV/cm by comparing the coherent and incoherent signals in the ABCD scheme described below and was confirmed with a calibrated thermopile. Using Si plates to attenuate the THz beam, it was found that the signals from the Si and GaAs devices were proportional to the THz electric field

up to this value. This result suggests that nonlinear effects, such as might result from field-driven intervalley transfer of photocarriers, are negligible because of field screening, at least at the relatively high THz frequencies produced by the laser ionized plasma source.

Fig. 2(c) shows the SOX to GaAs ratio spectrum obtained using a sampling pulse energy of 80 nJ. The ratio exhibits a slower fall off with increasing frequency than in Figs. 2(a) and 2(b), presumably because carrier scattering and energy relaxation are strongly affected by the hundred times larger carrier density. The overall ratio is also larger than in Figs. 2(a) and 2(b) because of the greater efficiency of field screening in GaAs than in Si. The peak to peak amplitude of the SOX device in Fig. 3(a) is about half of GaAs at the gating pulse energy of 80 nJ. Under these conditions the root mean square (RMS) noise current (THz beam blocked) was dominated by the thermal noise of the photoconducting gap with values of 15 and 50 fA/√Hz for SOX and GaAs respectively at 1 kHz compared with the current amplifier noise of 12 fA/√Hz. Hence the dynamic range (ratio of peak to peak signal to RMS background noise) of the two devices is very similar.

It is useful to compare the performance of the SOX device with electro-optic sampling and the recently developed technique of ABCD [9] under the same illumination geometry and pump and source conditions. Fig. 3 shows results for electro-optic detection in a 35 ± 2 μm thick (110) ZnTe crystal glued on an optically inactive 500 μm thick (100) ZnTe substrate. The probe energy was 80 nJ and the usual scheme of measuring the probe retardation with a polarising beam splitter, quarter wave optical bias and a pair of balanced photodiodes was employed. The crystal thickness was chosen to be small enough that the retardation is approximately linear in field up to ~1 MV/cm. Minima in the spectrum are expected near 13 THz and 29 THz because of the different dispersion of the THz phase velocity and optical group velocity but these are not clearly evident in Fig. 3b, possibly because of variations in crystal thickness. The small periodic undulations in the spectrum that are particularly apparent between 10 and 20 THz are due to reflections in the (110) ZnTe. The dynamic range is comparable with that obtained using photoconductive detection but the spectral response is significantly more complicated.

ABCD is based on the generation of second harmonic light by the mixing of THz and 800 nm probe pulses in an alternating bias field via the 3rd order optical nonlinearity of air. A pair of 3.75 mm diameter cylindrical copper electrodes with centre to centre spacing of 4.5 mm was square wave biased with a peak amplitude of 2 kV at 1 kHz and a probe pulse with an energy

of 8 μJ (below the threshold for plasma generation) was focused near the centre of the air-spaced electrode gap, co-linearly with the THz beam. The intensity of 400 nm light generated synchronously with the bias field and isolated using bandpass filters was recorded using a photomultiplier with a responsivity of 36 A/W and RMS dark current noise of 300 fA/√Hz. Figs. 3(a) and 3(b) show a time domain trace and spectrum which demonstrate that below 6 THz, photoconductive detection has superior dynamic range whilst between 6 and 20 THz the dynamic ranges are similar. The ABCD spectrum above 35 THz is not reproducible and is a noise related artefact arising from the highly nonlinear THz generation process. The noisy generation process is also evident in the low signal to noise ratio, defined as the RMS noise on the peak time domain signal to the RMS noise with the THz beam blocked. For the signals shown in Fig. 3(a), this ratio is approximately 150/√Hz for both ABCD and photoconductive detection.

In summary, we have demonstrated that ion implanted Si photoconductive receivers on Si substrates have a simple and ultrabroadband frequency response and a dynamic range similar to that obtainable with GaAs devices. Compared with electro-optic detection, the main advantages of Si devices apart from the absence of a restrahlen band are freedom from phase matching constraints and a linear response for THz fields approaching 1 MV/cm. Below 20 THz, Si devices have a comparable or superior (below ~7 THz) dynamic range to air-biased coherent detection and are simpler to set up. These features make Si detectors a particularly competitive choice for broadband TDTS with high THz fields. The specific device structure that we have described is not optimised, not least because the estimated size of the THz focal spot at the receiver is several hundred microns near 10 THz, which is significantly larger than the somewhat arbitrarily chosen 50 μm width of the photoconducting gap. A larger area, interdigitated structure [21] might be a better choice. Alternatively, the relatively low dispersion and absorption properties of the high resistivity Si substrate could be exploited by using counter-propagating gating and THz beams and a microlens etched into the substrate to reduce the THz focal size.

We thank the UK Engineering and Physical Science Research Council for funding under grant EP/J007595/1 and the Air Force Office of Scientific Research, Airforce Materiel Command, USAF under award number FA9550-15-1-0012.

References

[1] X.-C. Zhang and J. Xu, 'Introduction to THz wave photonics', Springer, New York (2010)

[2] P. R. Smith, D. H. Auston and M. C. Nuss, IEEE J. Quantum Electron. 24, 255 (1988)

[3] A. Sell, A. Leitenstorfer and R. Huber, Opt. Letts. 33, 2767 (2008)

[4] M. van Exter and D. R. Grischkowsky, IEEE Transactions on Microwave Theory and Techniques 38, 1684 (1990)

[5] F. G. Sun, G. A. Wagoner and X.-C. Zhang, Appl. Phys. Lett. 67, 1656 (1995)

[6] S. Kono, M. Tani and K. Sakai, Appl. Phys. Lett. 79, 898 (2001)

[7] A. Hussain and S. R. Andrews, Appl. Phys. Lett., 88, 143514 (2006)

[8] G. Wu and X.-C. Zhang, Appl. Phys. Lett. 68, 1604-7 (1996)

[9] X. Lu, N. Karpowicz, Y. Chen and X.-C. Zhang, Appl. Phys. Lett. 93, 261106 (2008)

[10] N. Katzenellenbogen, H. Chan and D. Grischkowsky, QELS Tech. Digest p155-6 (1993)

[11] S. R. Andrews, A. Armitage, P. G. Huggard and A. Hussain, Phys. Med. Biol. 47, 3705-3710 (2002)

[12] F. E. Doany, D. Grischkowsky and C.-C. Chi, Appl. Phys. Lett. 50, 460 (1987)

[13] N. Karpowicz, X. Lu and X.-C. Zhang, J. Mod. Optics 56, 1137 (2009)

[14] A. S. Barker, Phys. Rev. 132, 1474 (1963)

[15] M. Schubert, T. E. Tiwald and C. M. Herzinger, Phys. Rev. B61, 8187 (2000)

[16] M. C. Beard, G. M. Turner and C. A. Schmuttenmaer, J. Appl. Phys. 90, 5915 (2001)

[17] K. P. H. Liu and F. A. Hegemann, Appl. Phys. Lett. 78, 3478 (2001)

[18] T.-I. Jeon and D. Grischkowsky, Phys. Rev. Lett. 78, 1106 (1997)

[19] D. M. Riffe, JOSA B19, 1092 (2002)

[20] A. J. Sabbah and D. M. Riffe, Phys. Rev. B 66, 165217 (2002)

[21] F. Peter, S. Winnerl, S. Nitsche, A. Dreyhaupt, H. Schneider and M. Helm, Appl. Phys. Lett, 91, 081109 (2007)

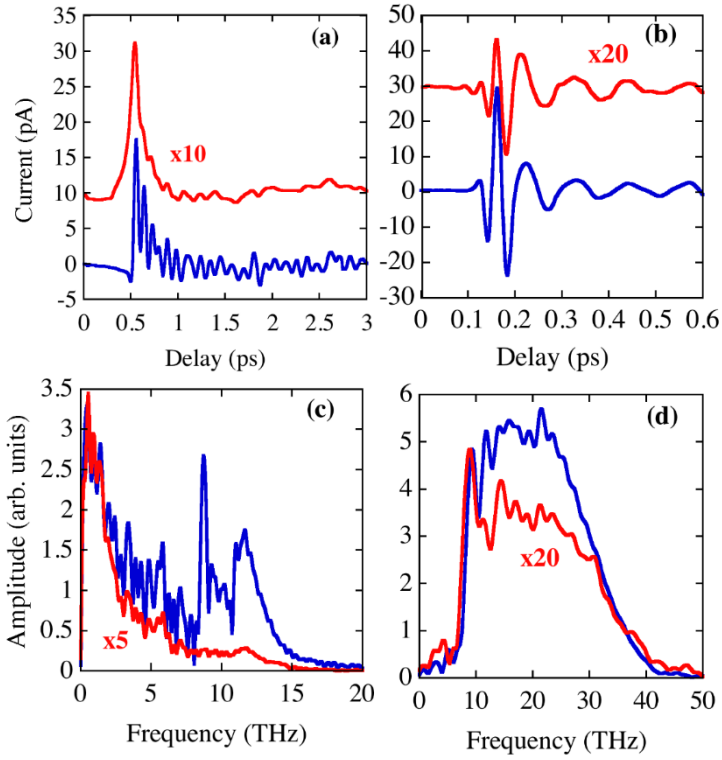

Fig. 1: (Colour online) (a), (b) Time domain signals for GaAs (lower traces) and SOX (upper) receivers obtained using InAs and a 30 μm thick GaSe crystal at a phase matching angle of 60° as THz sources respectively. The traces are offset for clarity. (c), (d) are corresponding spectra (upper curves: GaAs, lower : SOX).

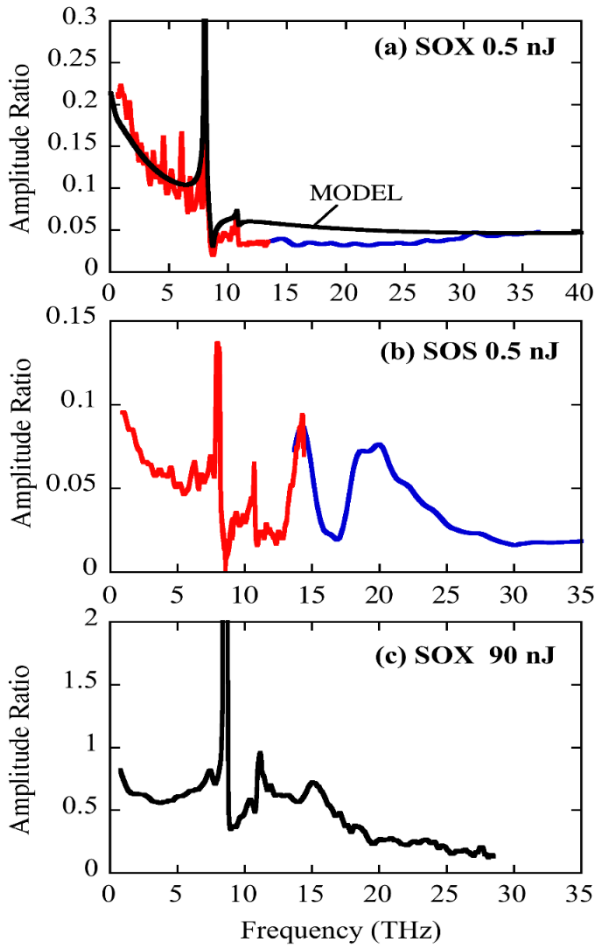

Fig. 2: (Colour online) (a), (b) Ratio of signal spectra of SOX and SOS receivers relative to that of GaAs at a sampling pulse energy of 0.5 nJ. Left hand portion (red) is obtained with InAs source, right hand (blue) with GaSe. The sharp peaks below 7 THz are due to a Fourier transform artefact. In (a) the black curve is a calculation described in the text. (c) SOX ratio at probe pulse energy of 80 nJ.

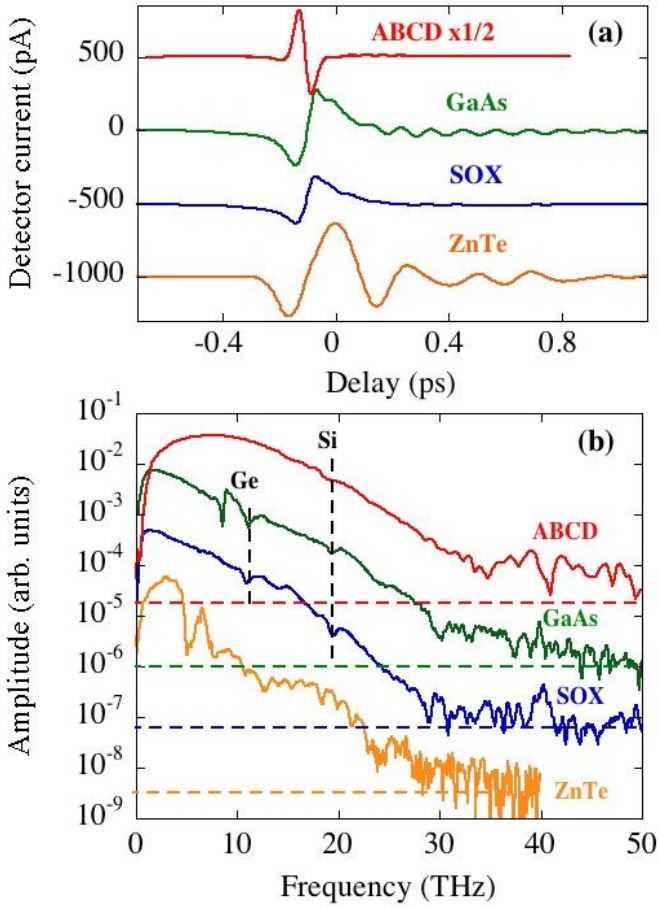

Fig. 3(a): (Colour online) Time domain detector signals obtained from a 2-colour laser ionized plasma source using different detectors. (b) The corresponding spectra and average background levels in the absence of a THz signal (horizontal dashed lines). The vertical dashed lines in (b) indicate frequencies of strong multiphonon absorption in Ge and Si filters. The ZnTe current scale in (a) can be converted into retardation by dividing by 10^4. The traces in both (a) and (b) are displaced vertically for clarity.